Journal of Sound and Vibration (1997) **202**(3), 395–415

CONTINUOUS CELL-TO-CELL MAPPING

B. TOMBUYSES

Université Libre de Bruxelles, *C.P.* 165, 50 *Avenue F.d. Roosevelt*, 1050 *Bruxelles*, *Belgium*

AND

T. ALDEMIR*

The Ohio State University, 206 *West* 18*th Avenue*, *Columbus*, *OH* 43210, *U.S.A.*

(*Received* 6 *December* 1995, *and in final form* 4 *November* 1996)

The cell-to-cell mapping technique (CCMT) is a numerical technique for the global analysis of non-linear dynamic systems and models system evolution as a Markov chain in discrete time. The computational feasibility of a continuous time version of CCMT is investigated using the van der Pol oscillator. The results show that while the continuous CCMT leads to large reduction in Markov model setup time and memory requirements as well as saving a large amount of computational time in the validation of the results with respect to the conventional CCMT, convergence to the asymptotic solution can be very slow. In these respect, the continuous CCMT approach is expected to be most effective as a scoping tool to determine the approximate location of the attractors.

1. INTRODUCTION

The cell-to-cell mapping technique (CCMT) is a numerical technique for the global analysis of non-linear dynamic systems [1, 2]. The CCMT models the evolution of dynamic systems as a mapping or probability of trajectory transitions between predefined sets of disjoint intervals (or cells) in the system state-space in discrete time. The cell-to-cell transition probabilities are determined from the system equations and a given time interval (mapping time step) and constitute the transition matrix of a Markov chain that yields the probability of finding the system within a given cell at a given time. A brief overview of the theoretical basis of CCMT is given in section 2. Some important features of CCMT are the following:

(1) The CCMT can be used to identify attractors consisting of a finite set of points, limit cycles, piecewise smooth surfaces or a volumes bounded by piecewise smooth closed surfaces, as well as strange attractors [1] much faster than direct integration. For example, it has been shown that the statistical properties of the strange attractor of a "stretch-contraction-reposition" map [3] can be determined by the CCMT 8 times faster than the direct integration method for the same accuracy. Similarly, it has been estimated that [4] the CCMT can identify the attractors of a third order system describing temporal xenon oscillations in a nuclear reactor 50–1000 times faster than direct integration.

(2) Since CCMT has no differentiability requirements on the governing equations (e.g., such as when using global perturbation of invariant manifolds [5]), it is perhaps the only technique other than direct integration that can be used for the global analysis of systems whose configuration may change as a function of system parameters (e.g., a process control system with on/off controls) or systems whose governing equations may be buried in a

* Correspondent

0022–460X/97/180395 + 21 $25.00/0/sv960835

complex, hard-wired simulator which has the system parameters as inputs (as is often encountered in practice).

(3) While numerous fast techniques have been proposed for the global analysis of non-linear systems (e.g., see references [6]–[13]), they are often impractical when the system has higher than two degrees of freedom. The CCMT has been successfully implemented to identify the attractors in the 4-dimensional state-space of a coupled two degree-of-freedom van der Pol system [14].

(4) Its probabilistic modeling of system dynamics makes CCMT naturally suited for the global analysis of systems with uncertainty on the system parameters and/or uncertainty on the observed system state. For example, the cells may represent the uncertainty in the monitored system state due to noise and/or the uncertainty in the system model parameters due to possible experimental error in their determination. Some applications of CCMT in probabilistic safety analysis are described in references [4, 15, 16].

The limitation of CCMT in implementation arises from computational requirements:

(5) Although the transition matrix for the Markov chain representing the system dynamics is generally very sparse, a fine state-space discretization scheme for adequately precise coverage of initial conditions of interest may not be computationally feasible due to excessive memory requirements even for relatively small systems.

(6) The choice of mapping time step and the cells are not completely independent of each other. This dependency between time and state-space discretization may require several trials with different discretization schemes to validate the results.

(7) Generation of the transition matrix can be computationally prohibitive if a large number of cells need to be used and several sets of calculations need to be performed to validate the results.

These aspects of CCMT are discussed in more detail in section 2. This paper investigates the feasibility of using a continuous time Markov model (section 3) rather than a discrete Markov chain for the determination of the system location in the state-space at a given time (section 2). The possibility of such an approach is originally mentioned in reference [17] and its potential in analyzing non-linear random systems is discussed in reference [19], however, the only application encountered in the available literature is a first order chemical system with a random coefficient [20]. This work shows that the continuous time approach gives very close results to the exact solution of the problem [20], but does not explore the computational advantages and disadvantages of the continuous CCMT with respect to the conventional or discrete CCMT. The main expected advantage of the continuous time approach is better control over the computer memory requirements. In addition, although a time step still needs to be chosen for the integration of the differential equations that constitute the continuous time Markov model, the choice of this time step is independent of the state-space discretization used and hence allows the use of an integration algorithm with variable stepsize. The computational features of the continuous time approach are investigated on the well-known van der Pol oscillator in sections 4 and 5. Section 6 gives the conclusions of the study.

2. AN OVERVIEW OF CCMT

Consider the system

$$\mathrm{d}\mathbf{x}/\mathrm{d}t = \mathbf{f}(\mathbf{x}, t), \tag{1}$$

where $\mathbf{x} \equiv \{x_1, x_2, \ldots, x_L\}$ is an L-vector whose components x_l are the dynamic variables, $\mathbf{f}(\mathbf{x}, t)$ is an L-vector representing the system equations and t is time. Now partition the

system-state space into sets of process variable magnitude intervals (cells) V_n such that

$$V_n \equiv \{x_l : a_{l,n_l} < x_l \leqslant a_{l,n_l+1};\ l = 1, \ldots, L\},$$

$$n \equiv n(n_1, n_2, \ldots, n_L); \quad n_l = 1, \ldots, N_l,\ l = 1, \ldots, L;\ n = 1, \ldots, N = N_1 N_2 \ldots N_L \tag{2}$$

and

$$\bigcup_{n=1}^{N} V_n = R, \quad V_m \cap V_n = \emptyset \qquad \text{for } m \neq n, \tag{3}$$

where R is the state-space region of interest and V_{N+1} represents the complement of R (sink cell). Figure 1 graphically illustrates such cells and the cell surfaces for a second order system with dynamic variable x_1 and x_2. The transition probability $g_{m,n}(\tau)$ from cell n to m can be found from [2]

$$g_{m,n}(\tau) = \begin{cases} \dfrac{1}{v_n} \displaystyle\int_{V_n} \mathrm{d}\mathbf{x}'\, e_m(\tilde{\mathbf{x}}(\mathbf{x}', \tau)) & \text{if} \quad V_n \in R, \\ 1 & \text{if} \quad n = m = N+1, \\ 0 & \text{if} \quad n = N+1 \quad \text{and} \quad m \neq N+1, \end{cases} \tag{4}$$

where v_n is the volume of V_n,

$$e_m(\mathbf{x}) \equiv \begin{cases} 1 & \text{if } \mathbf{x} \in V_m, \\ 0 & \text{otherwise,} \end{cases} \tag{5}$$

and

$$\tilde{\mathbf{x}}(\mathbf{x}', \tau) = \mathbf{x}' + \int_{k\tau}^{(k+1)\tau} \mathbf{f}(\mathbf{x}, t')\, \mathrm{d}t' \tag{6}$$

is the system location at time $(k+1)\tau$ in the state-space as obtained from the integration of equation (1), given that the system is at $\mathbf{x}'$ at time $k\tau$. The probability $p_n(k\tau)$ that the

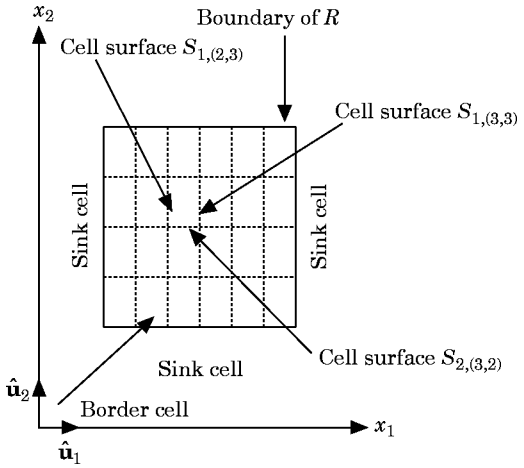

Figure 1. An example partitioning for a second order system with dynamic variables x_1 and x_2.

system is within cell n time $t = k\tau$ can be then obtained recursively from [1, 2]

$$\mathbf{p}((k+1)\tau) = \mathbf{G}\mathbf{p}(k\tau) \quad (k = 0, 1, 2 \ldots), \tag{7}$$

where $\mathbf{p}(k\tau)$ is a $N+1$-vector with elements $p_n(k\tau)$ and $\mathbf{G}$ is a $(N+1) \times (N+1)$ stochastic matrix with elements $g_{m,n}(\tau)$ $(n, m = 1, \ldots, N+1)$ (called the transition matrix). The τ is the mapping time step. Equations (2)–(6) show that equation (7) defines a Markov chain in discrete time.

In practice, the integral in equation (4) is approximated numerically to generate the transition matrix $\mathbf{G}$, which may require several trials with increasingly refined integration schemes to validate the approximation scheme used. However, whether a quadrature or a Monte Carlo scheme is used in the approximation of this integral, usually only a relatively few number of points can be selected as initial conditions from each cell for computational feasibility (see section 5) and, in this respect, it may be difficult to verify the adequacy of the integration scheme used. Similarly, several trials may be needed with different partitioning schemes to validate the results obtained from equation (7). For example, if τ is too small with respect to the time constants of equation (1) and the cell sizes, then the system may not move out of the cell it is in and subsequently equation (7) will not represent the system dynamics properly. A similar situation may also occur if τ is too large.

3. THE CONTINUOUS TIME CCMT AND ALGORITHM DEVELOPMENT FOR IMPLEMENTATION

In the limit $\tau \to 0$, equation (7) becomes [17, 18]

$$\frac{\partial p(\mathbf{x}, t)}{\partial t} + \nabla \cdot \mathbf{J}(\mathbf{x}, t) = 0, \qquad \mathbf{J}(\mathbf{x}, t) = p(\mathbf{x}, t)\mathbf{f}(\mathbf{x}, t), \tag{8}$$

where $p(\mathbf{x}, t)$ is the probability per unit volume of the state-space that the system is at $\mathbf{x}$ at time t and $\mathbf{J}(\mathbf{x}, t)$ represents the probability flow at point $\mathbf{x}$ at time t. Now integrate equation (8) over V_n. Using the definition of $p_n(t)$, i.e.,

$$p_n(t) = \int_{V_n} \mathrm{d}\mathbf{x}\, p(\mathbf{x}, t) \tag{9}$$

and the Stokes theorem to transform the volume integral of $\nabla \cdot \mathbf{J}(\mathbf{x}, t)$ to a surface integral, one obtains

$$\frac{\partial p_n(t)}{\partial t} + \int_{S_n} \mathrm{d}\mathbf{x}_s\, \hat{\mathbf{n}}(\mathbf{x}_s) \cdot \mathbf{J}(\mathbf{x}_s, t) = 0, \tag{10}$$

where S_n denotes the surface of V_n, $\mathbf{x}_s$ is a point on this surface and $\hat{\mathbf{n}}(\mathbf{x}_s)$ denotes the outward normal to S_n at $\mathbf{x}_s$. The surface integral in equation (10) can be written as

$$\int_{S_n} \mathrm{d}\mathbf{x}_s\, \hat{\mathbf{n}}(\mathbf{x}_s) \cdot \mathbf{J}(\mathbf{x}_s, t) = \int_{\substack{\hat{\mathbf{n}}(\mathbf{x}_s) \cdot \mathbf{J}(\mathbf{x}_s, t) > 0 \\ \mathbf{x}_s \in S_n}} \mathrm{d}\mathbf{x}_s\, \hat{\mathbf{n}}(\mathbf{x}_s) \cdot \mathbf{J}(\mathbf{x}_s, t) + \int_{\substack{\hat{\mathbf{n}}(\mathbf{x}_s) \cdot \mathbf{J}(\mathbf{x}_s, t) < 0 \\ \mathbf{x}_s \in S_n}} \mathrm{d}\mathbf{x}_s\, \hat{\mathbf{n}}(\mathbf{x}_s) \cdot \mathbf{J}(\mathbf{x}_s, t). \tag{11}$$

The first and second terms on the right hand side of equation (11) represent the probability outflow and inflow, respectively, per unit time for cell V_n. The probability inflow into V_n

can be expressed in terms of probability flow across the surfaces of the cells interfacing V_n, i.e.,

$$\int_{\substack{\hat{\mathbf{n}}(\mathbf{x}_s)\cdot\mathbf{J}(\mathbf{x}_s,\,t)<0\\ \mathbf{x}_s\in S_n}} d\mathbf{x}_s\,\hat{\mathbf{n}}(\mathbf{x}_s)\cdot\mathbf{J}(\mathbf{x}_s,\,t)=\sum_{n'}\int_{\substack{\hat{\mathbf{n}}(\mathbf{x}_s)\cdot\mathbf{J}(\mathbf{x}_s,\,t)<0\\ \mathbf{x}_s\in S_n\cap S_{n'}}} d\mathbf{x}_s\,\hat{\mathbf{n}}(\mathbf{x}_s)\cdot\mathbf{J}(\mathbf{x}_s,\,t), \tag{12}$$

where n' denotes the cells surrounding V_n. Under the assumptions that $p(\mathbf{x}, t)$ is uniformly distributed within each cell (also implicit in references [1] and [2]), i.e.,

$$p(\mathbf{x}, t)=p_n(t)/v_n \qquad \text{for } \mathbf{x}\in V_n, \tag{13}$$

and $p(\mathbf{x}, t)$ on a cell boundary is approximately equal to the $p_n(t)$ of the upstream cell (with respect to the probability flow), equations (9)–(13) yield

$$d\mathbf{p}/dt=\mathbf{Q}\mathbf{p}(t), \tag{14}$$

where $\mathbf{p}$ is a $N+1$-vector with elements $p_n(t)$ and $\mathbf{Q}$ is a $(N+1)\times(N+1)$ matrix (called the transition rate matrix) whose elements $q_{m,n}$ are determined from

$$q_{m,n}=\begin{cases} -\dfrac{1}{v_n}\displaystyle\int_{\substack{\hat{\mathbf{n}}(\mathbf{x}_s)\cdot\mathbf{f}(\mathbf{x}_s,\,t)>0\\ \mathbf{x}_s\in S_n}} d\mathbf{x}_s\hat{\mathbf{n}}(\mathbf{x}_s)\cdot\mathbf{f}(\mathbf{x}_s,\,t), & \text{if } m=n,\\[2ex] \dfrac{1}{v_n}\displaystyle\int_{\substack{\hat{\mathbf{n}}(\mathbf{x}_s)\cdot\mathbf{f}(\mathbf{x}_s,\,t)>0\\ \mathbf{x}_s\in S_n\cap S_m}} d\mathbf{x}_s\hat{\mathbf{n}}(\mathbf{x}_s)\cdot\mathbf{f}(\mathbf{x}_s,\,t), & \text{if } m\neq n. \end{cases} \tag{15}$$

Appendix A shows that $\Sigma_{m=1}^{N+1} q_{m,n}=0$. Appendix A also shows that: (1) $\mathbf{Q}$ has only eigenvalues with a non-positive real part, with at least one eigenvalue with zero real part (these zero real part eigenvalues are in fact equal to zero), and, (2) all zero eigenvalues are non-degenerated. Then for an autonomous system ($\mathbf{f}$ does not depend on t and $\mathbf{Q}$ is a constant matrix), the probability vector $\mathbf{p}(t)=e^{\mathbf{Q}t}\,\mathbf{p}(0)$ tends to an asymptotic solution.

For the mechanized construction of $\mathbf{Q}$, first enumerate the cells V_n using the following "lexicographic" scheme:

$$n\equiv n(n_1,\ldots,n_L)=1+(n_1-1)+(n_2-1)N_1+\cdots+(n_l-1)\prod_{l'}^{l-1}N_{l'}$$

$$+\cdots+(n_L-1)\prod_{l'}^{L-1}N_{l'}. \tag{16}$$

Then the surface integral $I_k(n_1, n_2, \ldots, n_L)$ on the face

$$S_{k,n}\equiv\{x_l\colon a_{l,n_l}\leqslant x_l\leqslant a_{l,n_l+1};\, l=1,\ldots,k-1,k+1,\ldots,L;\, x_k=a_{k,n_k}\}$$

$$(n=(n_1n_2,\ldots,n_L)) \tag{17}$$

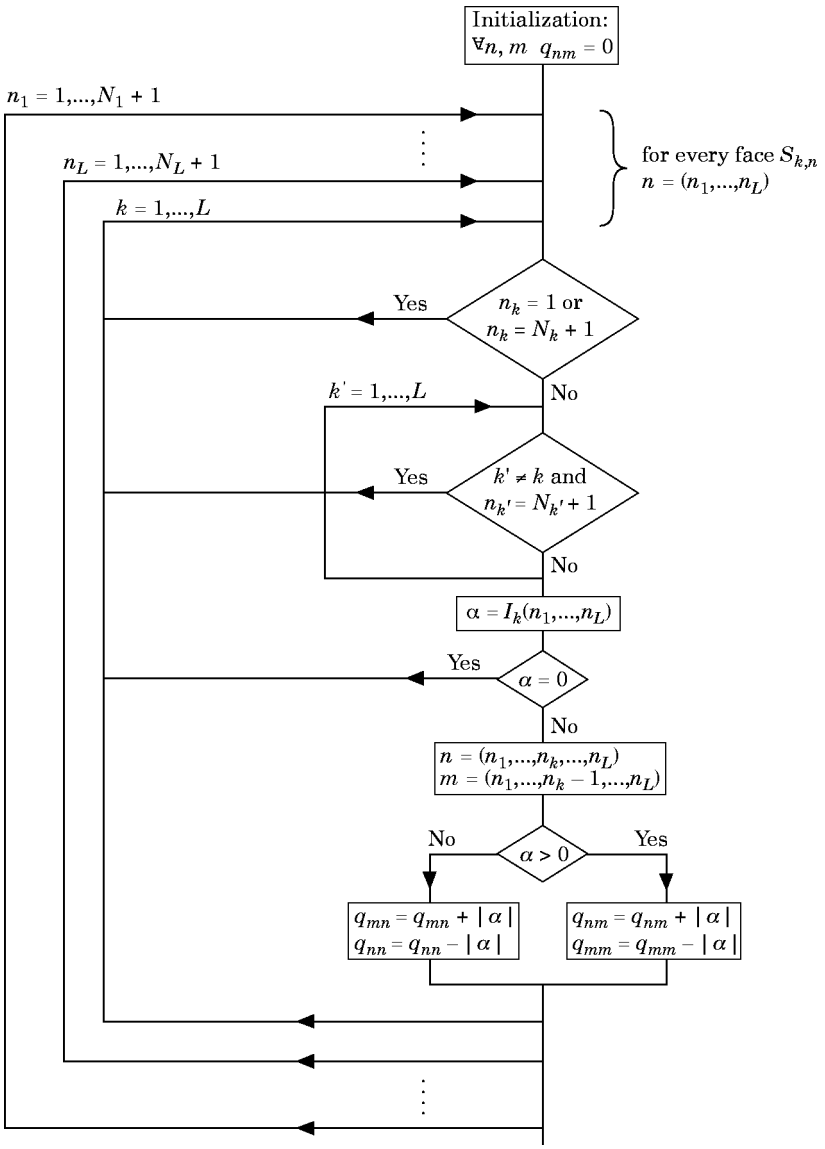

Figure 2. Flow chart for mechanized construction of the transition rate matrix **Q** (Method 1).

of the cell V_n can be written as

$$I_k(n_1,n_2,\ldots,n_L) = \int_{a_{1,n_1}}^{a_{1,n_1+1}} \mathrm{d}x_1 \cdots \int_{a_{k-1,n_{k-1}}}^{a_{k-1,n_{k-1}+1}} \mathrm{d}x_{k-1} \int_{a_{k+1,n_{k+1}}}^{a_{k+1,n_{k+1}+1}} \mathrm{d}x_{k+1} \cdots$$

$$\times \int_{a_{L,n_L}}^{a_{L,n_L+1}} \mathrm{d}x_L \, \hat{\mathbf{u}}_k \cdot \mathbf{f}(x_1, x_2, \ldots, x_{k-1}, a_{k,n_k}, x_{k+1} \cdots x_L), \tag{18}$$

where $\hat{\mathbf{u}}_k$ is the unit vector in the state-space in the k direction. If $I_k(n_1, n_2, \ldots, n_L)$ is positive, it represents a probability flow or transition from cell $m \equiv (n_1, \ldots, n_{k-1} \cdots n_L)$

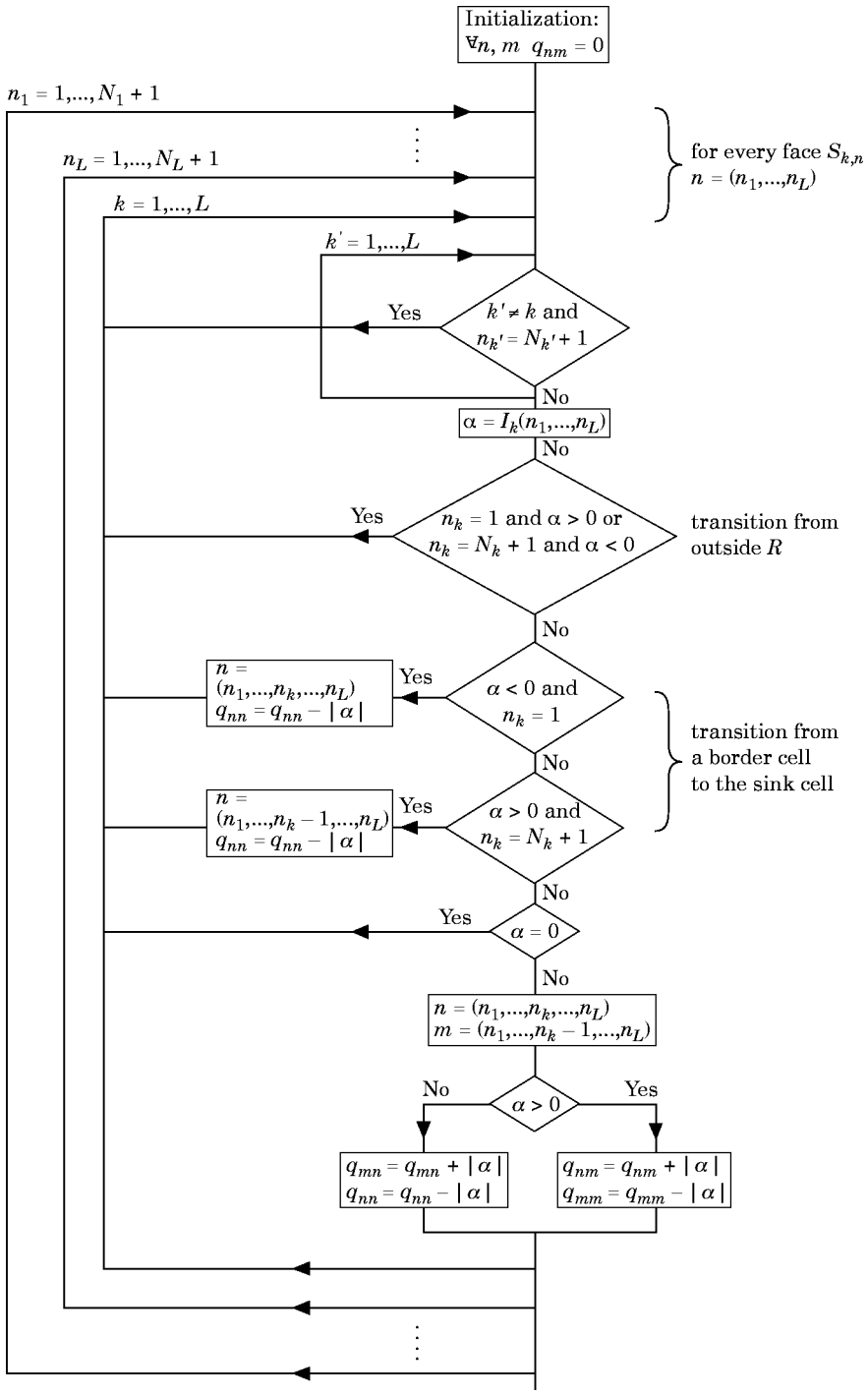

Figure 3. Flow chart for mechanized construction of the transition rate matrix **Q** (Method 2).

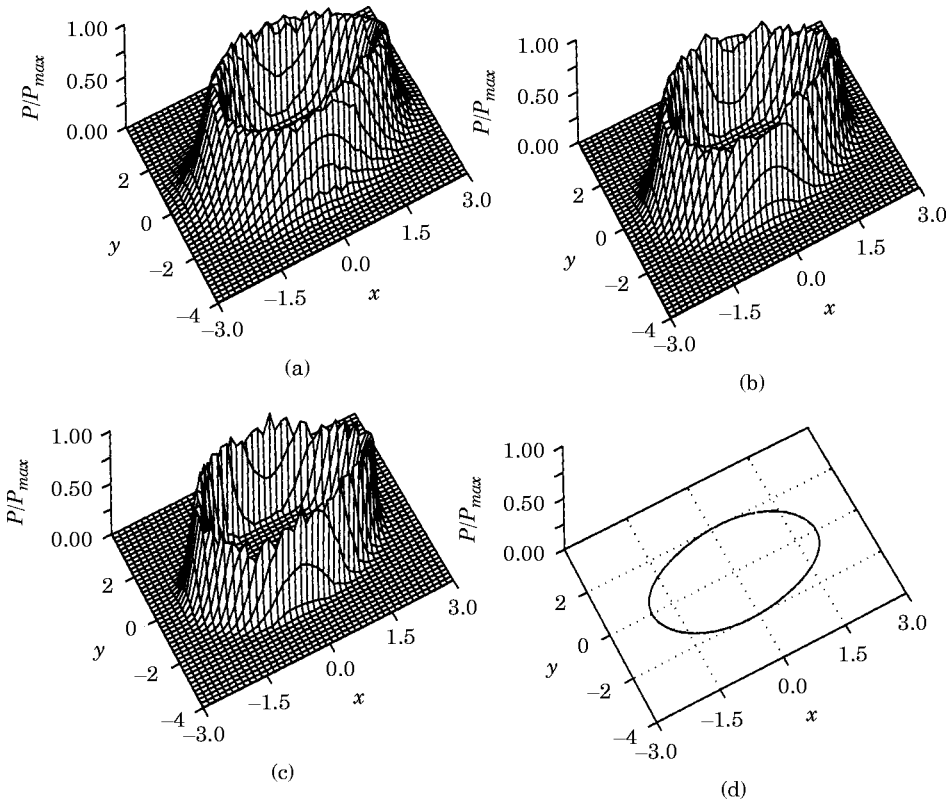

Figure 4. Relative probability distribution $P/P_{max} = p_n(\infty)/\max_n p_n(\infty)$ of the asymptotic behavior of the van der Pol oscillator for $\mu = 0{\cdot}1$ obtained by compactification: (a) using 50×50 cells; (b) using 100×100 cells; (c) using 200×200 cells; (d) exact solution.

to cell $n \equiv (n_1, \ldots, n_k, \ldots, n_L)$ and thus

$$q_{n,m} = I_k(n_1, n_2, \ldots, n_L)/v_m. \tag{19}$$

Conversely, if $I_k(n_1 n_2, \ldots, n_L)$ is negative, it represents a transition from cell $n \equiv (n_1, \ldots, n_k, \ldots, n_L)$ to cell $m \equiv (n_1, \ldots, n_{k-1}, \ldots, n_L)$ and

$$q_{m,n} = -I_k(n_1 n_2, \ldots, n_L)/v_n. \tag{20}$$

The diagonal elements of $\mathbf{Q}$ can be computed from the property $\Sigma_{m=1}^{N+1} q_{m,n} = 0$. The number of non-zero off-diagonal elements of $\mathbf{Q}$ is LN which compares very favorably to a possible maximum number of CN non-zero elements when using the approach described in reference [2], where $C = C_1 C_2 \ldots C_L$ is the number of quadrature points used in the numerical evaluation of the integral in equation (4) with C_l, $l = 1, \ldots, L$ denoting the number of partitions used in each l direction for the selection of the quadrature points.

At this point it should be indicated that, as V_n become infinitely small, the non-zero $q_{n,m}$ increase to infinite values. On the other hand, $p_n(t)$ also tend to zero with decreasing V_n, except for V_n that contain the attractor. These V_n will eventually become the support of the attractor as they themselves go to zero and the probability density in a cell n, $p_n(t)/v_n$, will tend to a Dirac delta distribution over this support. This situation is illustrated by using a simple example in Appendix B. Also, reference [20] shows that for the first order

system under consideration in reference [20], the solution of equation (14) exists and is unique. However, a general proof of convergence for continuous time CCMT (i.e., finding the general sufficient and necessary conditions to assure the convergence, the norm that can be used as a convergence criterion, etc.), is a mathematically very difficult problem and is beyond the scope of this paper. It should be also mentioned that while numerical roundoff may, in principle, lead to numerical problems with decreasing V_n and thus increasing transition rates, the V_n used in most practical problems are not expected to be small enough for such roundoff effects to have appreciable impact on the results.

Figures 2 and 3 show the flowcharts for two possible algorithms for the mechanized partitioning of the state-space and construction of **Q**. In both approaches, a cell face is characterized by the $L+1$ numbers $n_1, n_2, \ldots, n_L$ and k which indicates the axis orthogonal to the cell surface $S_{k,n(n_1,n_2,\ldots,n_L)}$ (see Figure 1). If $\alpha = I_k(n_1, \ldots, n_L)$ is >0, the transition is from cell $m \equiv (n_1, \ldots, n_{k-1}, \ldots, n_L)$ to the cell $n \equiv (n_1, \ldots, n_k, \ldots, n_L)$. If α is <0, the transition is from cell n to cell m. The only difference between Method 1 (Figure 2) and Method 2 (Figure 3) is the way the border cells (see Figure 1) are handled to prevent loss of ergodicity of equation (14), which may arise due to the well-known problem of false diffusion. The different tests in Figures 2 and 3 examine the situation at these border cells. In Method 2, transitions into $\bar{R}$ from the border cells are computed and redistributed to the cells of the domain as loss terms by a normalization operation. In Method 1, these transitions are not taken into account and the probability of transition

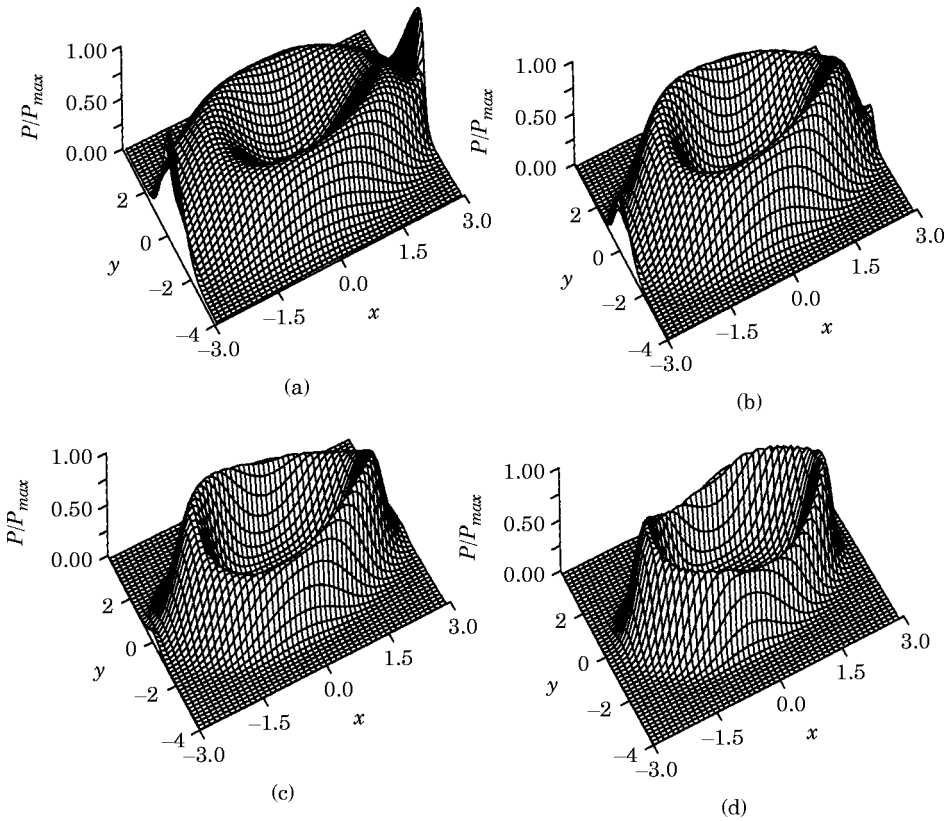

Figure 5. Relative probability distribution $P/P_{max} = p_n(\infty)/\max_n p_n(\infty)$ of the asymptotic behavior of the van der Pol oscillator for $\mu = 0{\cdot}1$ obtained by Method 1 using: (a) 50×50 cells; (b) 100×100 cells; (c) 200×200 cells; (d) 400×400 cells.

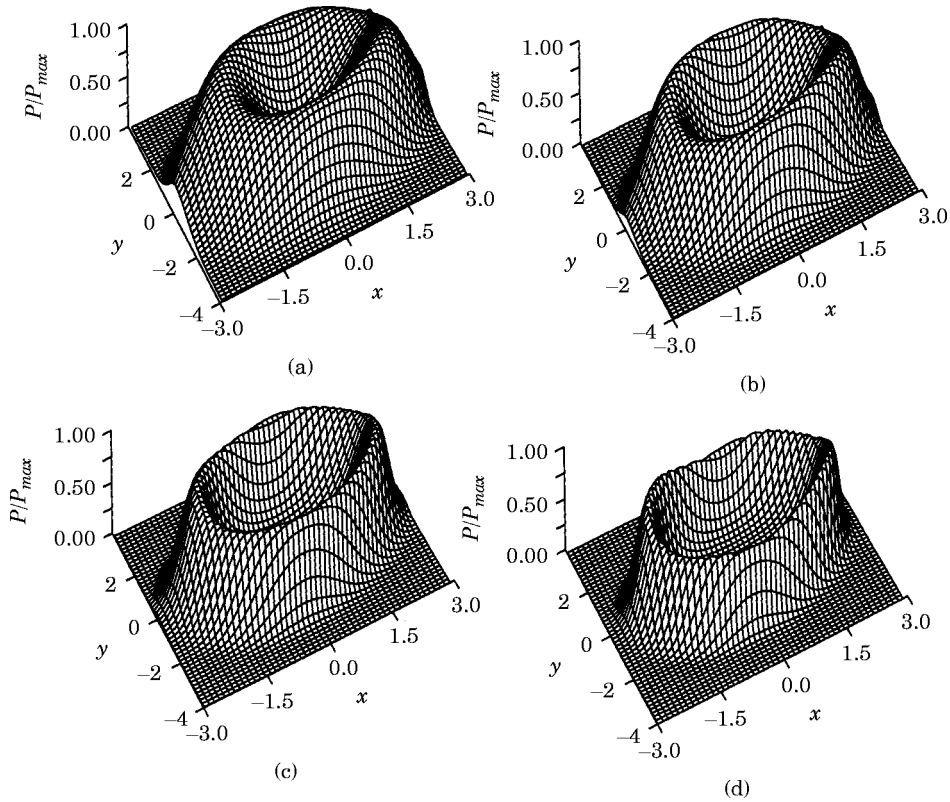

Figure 6. Relative probability distribution $P/P_{max} = p_n(\infty)/\max_n p_n(\infty)$ of the asymptotic behavior of the van der Pol oscillator for $\mu = 0{\cdot}1$ obtained by Method 2 using: (a) 50×50 cells; (b) 100×100 cells; (c) 200×200 cells; (d) 400×400 cells.

from the border cells into R are assumed to be zero. Another approach that can be used is the "compactification" of the domain of the dynamical variables by the transformation of the variables $\mathbf{x}$ into variables $\mathbf{y}$ which have a bounded domain [17]. The resulting system $\mathrm{d}\mathbf{y}/\mathrm{d}t = \mathbf{g}(\mathbf{y}, t)$ is dynamically equivalent to $\mathrm{d}\mathbf{x}/\mathrm{d}t = \mathbf{f}(\mathbf{x}, t)$ if the transformation preserves the number and the nature of singular points. In these situations Methods 1 and 2 become identical. The numerical implications of these approaches are discussed in section 4.

4. APPLICATION: THE VAN DER POL OSCILLATOR

For the illustration of the continuous CCMT, we will use the classical problem of van der Pol that has been considered earlier in the implementation of the discrete CCMT [1]. The system equations are

$$\mathrm{d}x/\mathrm{d}t = y, \qquad \mathrm{d}y/\mathrm{d}t = \mu(1 - x^2)y - x, \quad \mu > 0. \tag{21}$$

It is well known that equation (21) has a stable limit which all the trajectories approach, except those starting at the origin which maps onto itself. For compactification, the transformation $(x, y) \rightarrow (\rho = r/(1 + r), \theta)$ has been used where r, θ are the polar

co-ordinates. The new system is

$$\frac{\mathrm{d}\rho}{\mathrm{d}t} = \frac{\rho}{1-\rho}\,\mu \sin^2\theta((1-\rho)^2 - \rho^2\cos^2\theta),$$

$$\frac{\mathrm{d}\theta}{\mathrm{d}t} = \mu \sin\theta\cos\theta\,\frac{1}{(1-\rho)^2}((1-\rho)^2 - \rho^2\cos^2\theta) - 1, \tag{22}$$

where the range for ρ is [0, 1] and the range for θ is $[0, 2\pi]$. The integral in equation (4) was evaluated by quadratures using evenly spaced subintervals in each cell. A variable stepsize fourth order Runge–Kutta method was used for integrating equation (4) as well as equation (14), using uniform probability distribution in R as the initial condition. Figure 4 compares the results obtained for $\mu = 0{\cdot}1$ with the compactification approach using 50×50, 100×100, 200×200 cells to the exact solution. The results have been mapped back to the x–y plane. Convergence of the asymptotic solution of equation (7) was determined using the criterion

$$|p_n(k+1) - p_n(k)| \leqslant \epsilon p_n(k) + \delta, \qquad \forall V_n \in R,$$

where $\epsilon = 10^{-3}$ and $\delta = 10^{-9}$. Convergence of the asymptotic solution of equation (14) was

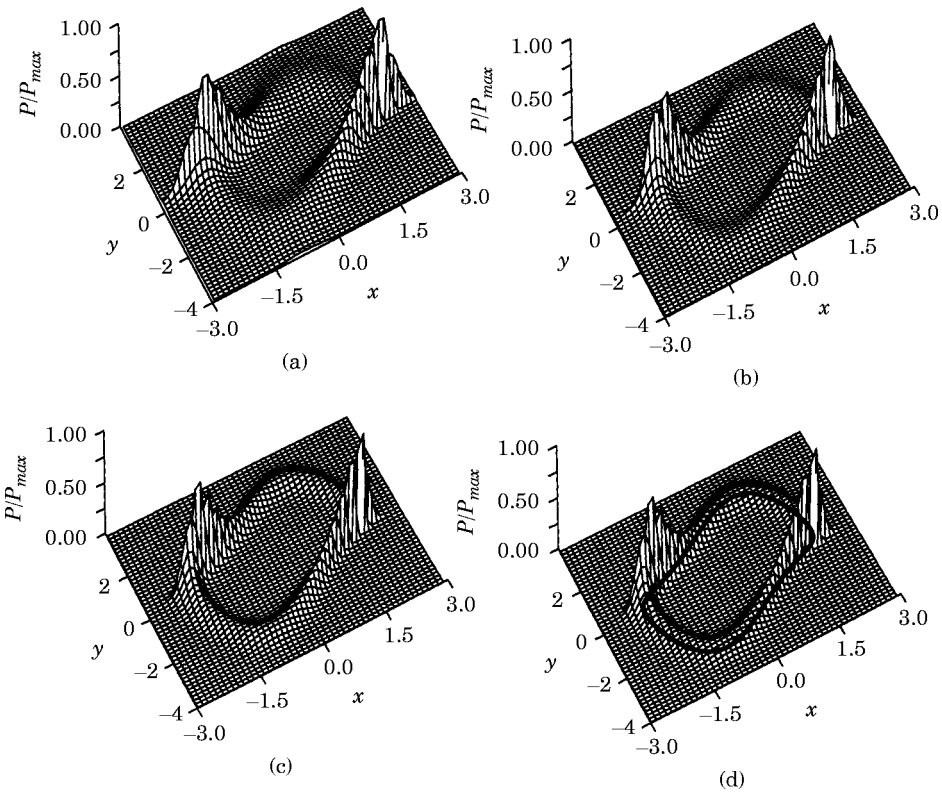

Figure 7. Relative probability distribution $P/P_{max} = p_n(\infty)/\max_n p_n(\infty)$ of the asymptotic behavior of the van der Pol oscillator for $\mu = 1{\cdot}0$ obtained by Method 1 using: (a) 50×50 cells; (b) 100×100 cells; (c) 200×200 cells; (d) 400×400 cells.

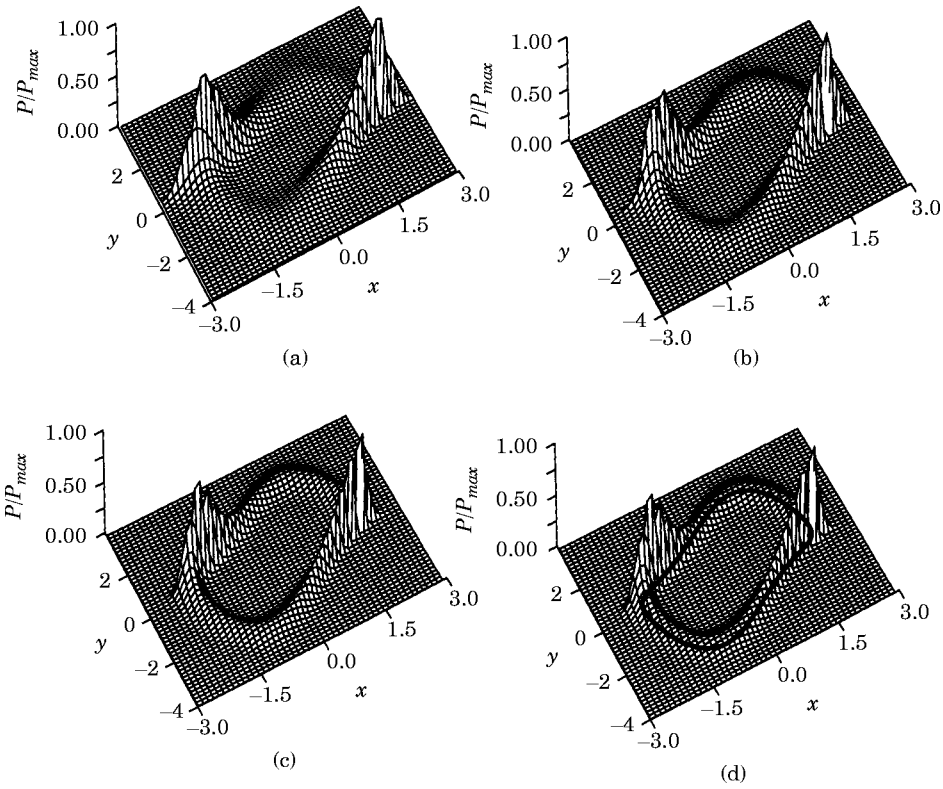

Figure 8. Relative probability distribution $P/P_{max} = p_n(\infty)/\max_n p_n(\infty)$ of the asymptotic behavior of the van der Pol oscillator for $\mu = 1{\cdot}0$ obtained by Method 2 using: (a) 50×50 cells; (b) 100×100 cells; (c) 200×200 cells; (d) 400×400 cells.

determined when for two successive times t and t', one has

$$|p_n(t') - p_n(t)| \leqslant \epsilon p_n(t) + \delta, \qquad \forall V_n \in R,$$

again for $\epsilon = 10^{-3}$ and $\delta = 10^{-9}$.

Figures 5 and 6 show the results for Method 1 and Method 2, respectively, using 50×50, 100×100, 200×200 and 400×400 cells. All the three methods give the periodic orbit as an attractor but not the origin since it is an unstable stationary point. Note that a similar problem can also appear for CCMT, depending on the choice of τ and the number of quadrature points per cell. Figures 4–6 show that the most accurate results are obtained

TABLE 1

Computation times to obtain the asymptotic solution for van der Pol oscillator using the continuous CCMT

Method	CPU time (s) for N cells				CPU time/Smallest CPU time for N cells			
	50^2	100^2	200^2	400^2	50^2	100^2	200^2	400^2
"Compactification"	282·69	1001·33	8047·80	—	21·38	11·04	11·83	—
1	20·99	192·46	1803·87	12 069·04	1·59	2·12	1·84	2·23
2	13·22	90·70	680·35	5412·13	1	1	1	1

TABLE 2

A comparison of some computational features of the CCMT and the continuous CCMT for the asymptotic solution of the van der Pol oscillator with $\mu = 1{\cdot}0$

Case	Method	N	C	τ	M_{max}	T_{matrix}	T_{total}
1	CCCMT	20^2	—	—	794	0·01	0·54
2	CCMT	20^2	4	0·1	1021	0·20	1·45
3	CCCMT	50^2	—	—	4984	0·01	11·54
4	CCMT	50^2	4	0·1	7236	1·14	3·52
5	CCCMT	100^2	—	—	19 968	0·04	197.65
6	CCMT	100^2	4	0·1	30 300	4·56	57·16
7	CCMT	100^2	4	1·0	29 611	11·61	120·12
8	CCMT	100^2	4	10·0	40 327	67·78	—
8b	CCMT	100^2	4	9·9	40 003	67·34	193·27
8c	CCMT	100^2	4	10·1	40 267	68·68	185·97
9	CCMT	100^2	4	100·0	40 120	633·98	668·97
10	CCMT	100^2	16	0·1	37 319	72·96	128·45
11	CCMT	100^2	16	1·0	37 073	187·12	299·46
12	CCMT	100^2	16	10·0	54 099	1097·50	1352·56
13	CCMT	100^2	16	100·0	53 262	10 217·81	10 247·96

CCMT, cell to cell mapping technique; CCCMT, continuous cell to cell mapping technique; N, number of cells used; C, number of subcells or quadrature points used in the approximation of the integral in equation (6); τ, mapping step size (see equation (6)) in seconds; M_{max}, number of non-zero elements in the transition matrix **G** or the transition rate matrix **Q**; T_{matrix}, computational processing time used to generate the transition matrix **G** or the transition rate matrix **Q** in s; T_{total}, total computational processing time used to obtain the solution in s.

by the "compactification" method. For a small number of cells, Figure 5 shows that Method 1 leads to some deformation near the boundary of R, because Method 1 does not account for transitions going out of domain R. Since the cell probabilities in Figures 4–6 are proportional to the time spent in the cells, cells with high probabilities correspond to the low velocity regions along the system trajectory. This phenomenon is more visible for $\mu = 1$ as can be seen from Figures 7 and 8 which have been obtained using Method 1 and Method 2, respectively.

Table 1 gives the computation times for the cases considered in this study. While Table 1 shows that Method 2 is much faster than either Method 1 or the "compactification" method for a given number of cells, a comparison of Figures 4–6 shows that the "compactification" method yields as much detail with 50×50 cells as Method 2 does with 400×400 cells. In this respect, Table 1 shows that the "compactification" method can be about 20 times faster than Method 2 for a given accuracy of results. It should be indicated, however, that this possible computational advantage of the "compactification" method is contingent upon the choice of the transformation. For example, if the polar co-ordinates for the example system above were chosen with the origin far from the region of interest for the system, the results would be very poor.

5. COMPARISON OF COMPUTATIONAL FEATURES OF CONTINUOUS CCMT TO DISCRETE CCMT

In order to investigate the computational features of continuous CCMT with respect to the discrete CCMT, a set of parametric studies were carried out for the example system with $\mu = 1{\cdot}0$ using a different number of cells (i.e., N), quadrature points or subcells C for the approximation of the integral in equation (6) and a different mapping step size τ (see equation (6)). The results are shown in Table 2. The predicted asymptotic behavior of the system for Cases 1–12 (see Table 2) as well as the exact solution are shown in

Figures 9–11. Cases 1–12 in Figures 9–11 have been plotted using the "local maxima"; i.e., selecting the cells with probabilities higher than the surrounding cells. The lack of convergence for Case 8 is attributed to the possible cyclicity of the transition matrix for Case 8. A solution to such a convergence problem is to use a convergence criterion based on the Cesaro sums instead of the criteria given in section 4. The following observations are made from Table 2 and Figures 9–11:

(1) *Continuous CCMT leads to large reduction in Markov model setup time*. Comparison of T_{matrix} times in Table 2 shows that the generation of the transition rate matrix **Q** (see equation (14)) is 0·20/0·1 = 20 to 10217·81/0·04 = 255 445 times faster than the generation of the transition matrix **G** (see equation (7)), depending on the partitioning scheme and the number of subcells used in the approximation of the integral in equation (4). Comparison of Cases 6–9 with Cases 10–13 in Table 2 also shows that model construction time for discrete CCMT increases very rapidly with the number of subcells or quadrature points used in the approximation of the integral in equation (6).

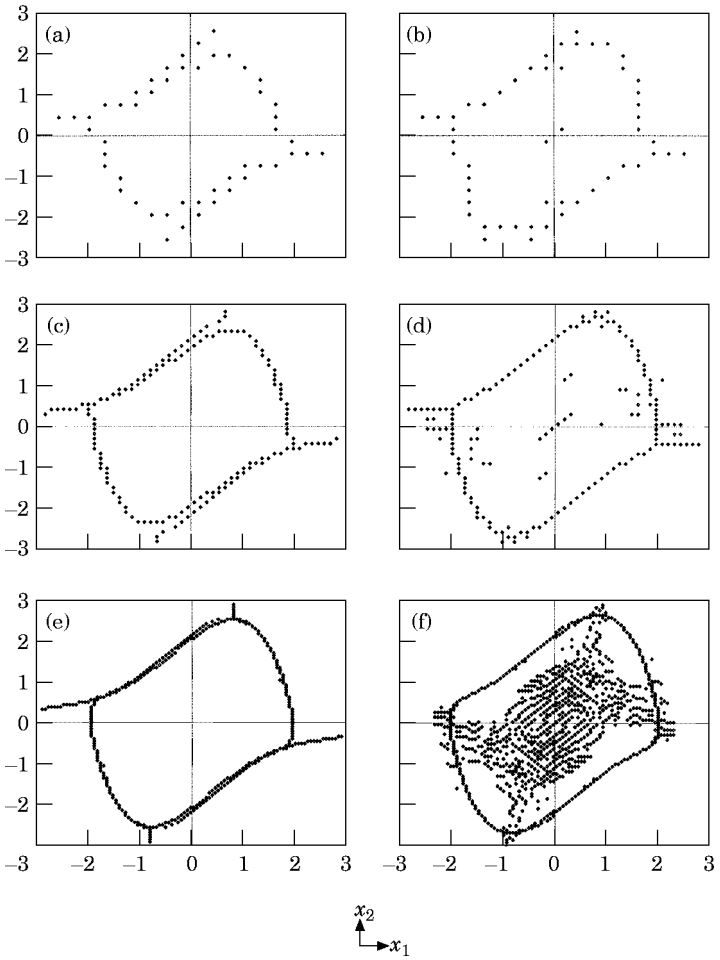

Figure 9. Asymptotic solutions of the van der Pol oscillator with $\mu = 1{\cdot}0$ for Cases 1–6 obtained from the local maxima: (a) Case 1 (CCCMT 20 × 20 cells); (b) Case 2 (CCMT 20 × 20 cells, $\tau = 0{\cdot}1$ s); (c) Case 3 (CCCMT 50 × 50 cells); (d) Case 4 (CCMT 50 × 50 cells, $\tau = 0{\cdot}1$ s); (e) Case 5 (CCCMT 100 × 100 cells); (f) Case 6 (CCMT 100 × 100 cells, $\tau = 0{\cdot}1$ s).

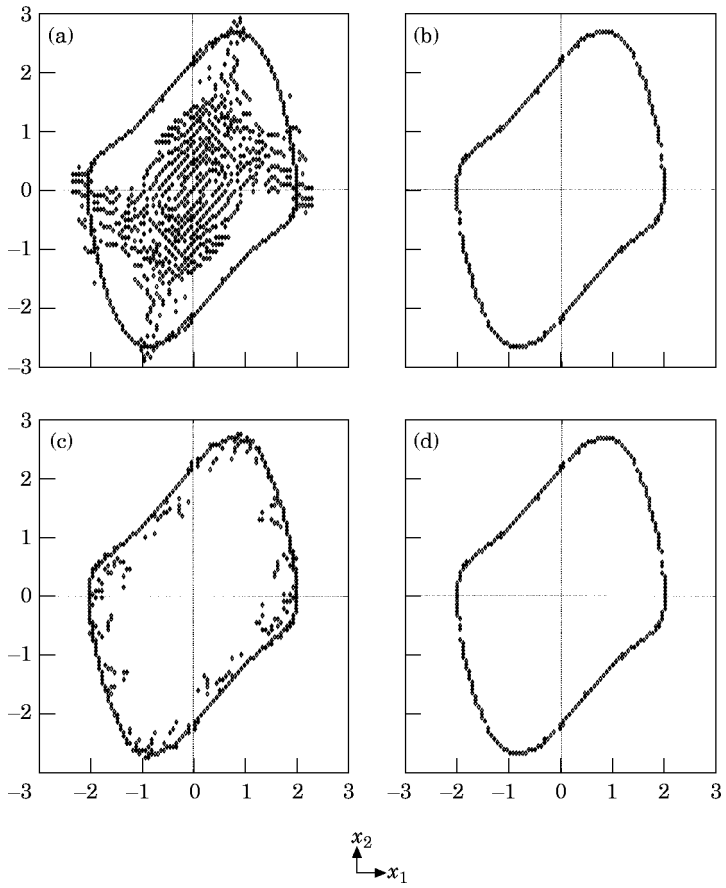

Figure 10. Asymptotic solutions of the van der Pol oscillator with $\mu = 1{\cdot}0$ for Cases 6–9 obtained using the local maxima: (a) Case 6 ($\tau = 0{\cdot}1$ s); (b) Case 7 ($\tau = 1{\cdot}0$ s); (c) Case 8 ($\tau = 10{\cdot}0$ s); (d) Case 9 ($\tau = 100{\cdot}0$ s).

(2) *Continuous CCMT leads to large reduction in memory requirements*. For example, for Cases 5 and 13 in Table 2 the reduction is by a factor of $53\,262/19\,968 = 2{\cdot}67$.

(3) *Continuous CCMT saves a large amount of computational time in the validation of the results*. The time savings originate from the fact that the discrete CCMT requires experimentation with τ and the number of subcells used in the approximation of the integral in equation (4) to validate the results for a given partitioning scheme. Table 2 shows that the total time used to validate the results for the 100×100 partitioning scheme (i.e., the sum of T_{total} for Cases 6–13) is about 13 350 s which is $13\,350/197{\cdot}65 = 67{\cdot}5$ times larger than T_{total} for Case 5.

(4) *For comparable accuracy on the predicted asymptotic system behavior, continuous CCMT can still be computationally advantageous*. For example, a fairly conservative choice of Case 10 results in Figure 11 as being comparable to Case 5 results in Figure 9 regarding accuracy and the corresponding data in Table 2 indicate that while the total computational time to obtain the results increases by about $197{\cdot}65/128{\cdot}45 = 1{\cdot}54$, the reduction in memory requirements is by a factor of $37\,319/19\,968 = 1{\cdot}87$. For a more favorable choice of Case 11 in Figure 11 for comparison, results instead of Case 10, Table 2 shows that both the total computational time and memory requirements are lower for continuous CCMT by a factor of $299{\cdot}46/197{\cdot}65 = 1{\cdot}52$ and $37\,073/19\,968 = 1{\cdot}86$, respectively.

On a more negative note, Table 2 and Figures 9–11 indicate the following difficulties with the continuous CCMT:

(5) *Convergence of equation* (14) *to the asymptotic solution is very slow*. Inspection of the T_{matrix} and T_{total} data in Table 2 shows that while the model generation times are much smaller than the discrete CCMT, the total computational time to obtain the results can be much longer.

(6) *Equation* (14) *may only have a trivial asymptotic solution*. This situation is relevant to systems where the dynamic variables are defined on an unbounded domain. Since there is always a finite transition probability between adjacent cells according to equation (15), the sink cell is reachable from all the cells in this situation and hence all the cells eventually lead to the sink cell. In that respect, approximations may need to be used such as was done in this study (i.e., Method 1 and Method 2 described in section 3). However, such a problem does not occur if compactification is possible.

(7) *Continuous CCMT may erroneously predict paths to the sink cell as part of the attractor*. Comparison of Cases 1, 3 and 5 in Figure 9 to the exact asymptotic solution in Figure 11 shows that the continuous CCMT predicts 4 paths to the sink cell which should not be there. Again, this phenomenon originates from the sink cell being reachable from all the cells when the dynamic variables are defined on an unbounded domain. The paths indicate the path of probability flow out of R. Note that such paths may also exist

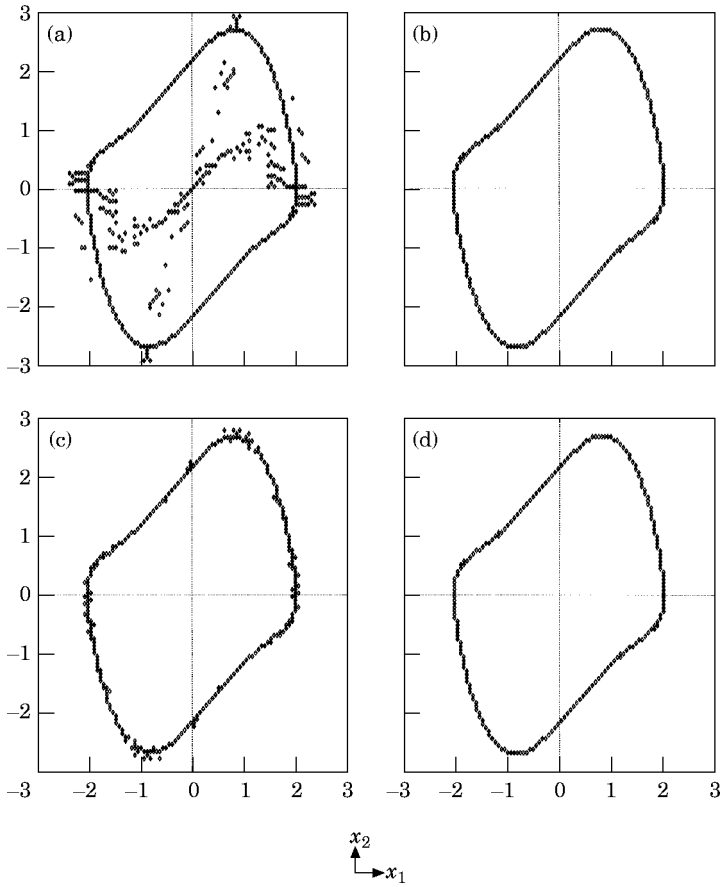

Figure 11. Exact and asymptotic solutions of the van der Pol oscillator with $\mu = 1{\cdot}0$ for Cases 10–12 obtained using the local maxima: (a) Case 10 ($\tau = 0{\cdot}1$ s); (b) Case 12 ($\tau = 10{\cdot}0$ s); (c) Case 11 ($\tau = 1{\cdot}0$ s); (d) exact solution.

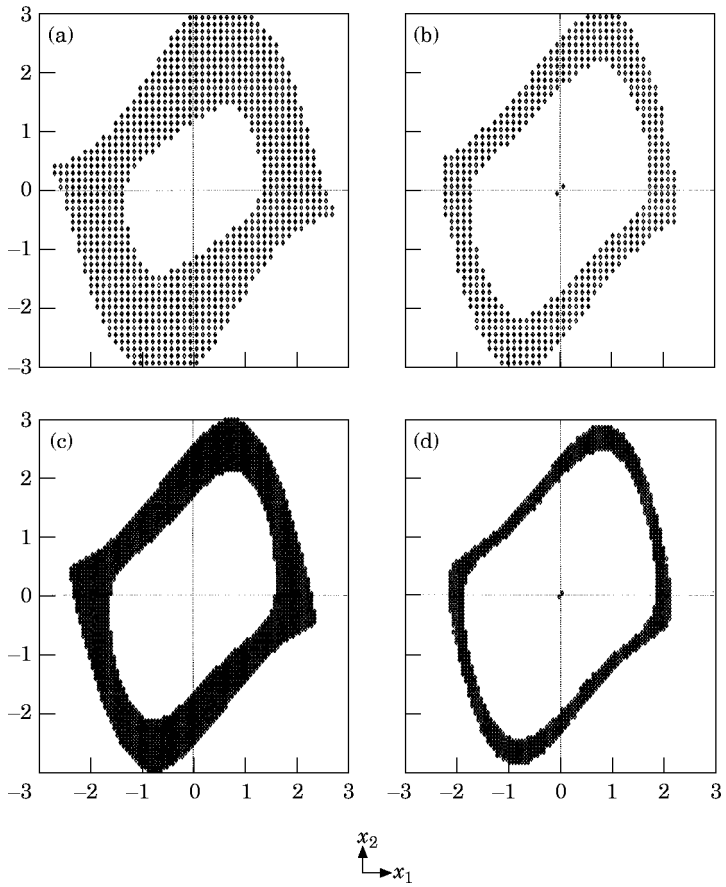

Figure 12. Asymptotic solutions of the van der Pol oscillator with $\mu = 1{\cdot}0$ for Cases 3–6 obtained using a minimum cutoff on $p_n(t)$: (a) Case 3 (Continuous CCMT, 50×50 cells); (b) Case 4 (CCMT, 50×50 cells, 4 subcells, $\tau = 0{\cdot}1$ s); (c) Case 5 (continuous CCMT, 100×100 cells); (d) Case 6 (CCMT, 100×100 cells, 4 subcells, $\tau = 0{\cdot}1$ s).

for coarse mesh partitionings with CCMT for small τ (i.e., Cases 2 and 4 in Figure 9) which may lead to a similar connectivity between the cells. Comparison of Case 6 results in Figure 10 to Cases 7–9 results show that while the paths start disappearing with the refinement of the partitioning and also with increasing τ for the discrete CCMT, Cases 1, 3 and 5 in Figure 9 show that the paths remain for the continuous CCMT irrespective of the partitioning scheme used. Since the probability of finding the system on the attractor is much higher than on these paths, it is possible to remove the paths by not plotting points with probabilities lower than some specified value as shown for Cases 3–6 in Figure 12, instead of plotting the local maxima as was done in Figures 9–11. However, this approach may lead to more blurring or "fattening" of the attractor using continuous CCMT than CCMT as again shown for Cases 3–6 in Figure 12.

6. CONCLUSION

This study investigates the computational features of the continuous CCMT using the van der Pol oscillator. The results of the study show that the continuous CCMT leads to a large reduction in Markov model setup time and in memory requirements and can be

computationally advantageous with respect to the discrete CCMT for comparable accuracy on the predicted asymptotic system behavior for some choices of the mapping time step τ and state-space partitioning scheme. On the other hand, the results of the study also show that convergence of the continuous CCMT to the asymptotic solution is very slow, sometimes requiring the use of additional approximations, as well as the improvement of the accuracy of the results with increasing refinement in partitioning. In these respect, the continuous CCMT approach is expected to be most effective as a scoping tool to determine the approximate location of the attractors. Then the discrete CCMT can be used to refine the results without excessive experimentation on the choice of the partitioning scheme and the mapping time step τ. It should be also indicated that both the discrete CCMT and the continuous CCMT are different discretization methods to solve equation (14) and more effective other discretization methods may be possible. Similarly, it may be possible to find more effective integration algorithms to alleviate the problem of slow convergence of equation (14).

REFERENCES

1. C. S. Hsu 1987 *Cell-to-Cell Mapping*: *A Method for Global Analysis of Non-Linear Systems*. New York: Springer-Verlag.
2. M. Belhadj and T. Aldemir 1995 *Journal of Sound and Vibration* **181**, 687–707. The cell-to-cell mapping technique and Chapman–Kolmogorov representation of system dynamics.
3. C. S. Hsu and M. C. Kim 1986 *Journal of Statistical Physics* **38**, 735–761. Statistics of strange attractors by generalized cell mapping.
4. M. Belhadj and T. Aldemir 1991 *Transactions of the American Nuclear Society* **64**, 291–293. Probabilistic analysis of asymptotic reactor dynamics and the cell-to-cell mapping technique.
5. S. Wiggings *Global Bifurcations and Chaos*: *Analytical Methods*. New York: Springer-Verlag.
6. T. Kapitaniak 1991 *Chaotic Oscillations in Mechanical Systems*. Manchester, U.K.: Manchester University Press.
7. R. H. Rand and D. Armbruster 1987 *Perturbation Methods*, *Bifurcation Theory and Computer Algebra*. New York: Springer-Verlag.
8. F. H. Busse and M. Sieber 1991 *International Series of Numerical Mathematics* **97**, 79–92. Regular and chaotic patterns of Rayleigh-Bernard convection.
9. J. P. Eckmann and D. Ruelle 1985 *Reviews of Modern Physics* **57**, 617–656. Ergodic theory of chaos and strange attractors.
10. C. Froeschle 1984 *Journal de Mechanique Theorique et Appliquee*, Numero special supplement, 101–132. The Lyapunov characteristic exponents and applications.
11. D. Ruelle 1989 *Elements of Differentiable Dynamics and Bifurcation Theory*. San Diego, California: Academic Press, Inc.
12. T. J. Garratt, G. Moore and A. Spence 1991 *International Series of Numerical Mathematics* **97**, 129–134. Two methods for the numerical detection of Hopf bifurcations.
13. D. Ruelle 1987 *Chaotic Evolution and Strange Attractors*: *The Statistical Analysis of Time Series for Deterministic Nonlinear Systems*. Cambridge, U.K.: Cambridge University Press.
14. J. X. Xu, R. S. Guttalu and C. S. Hsu 1985 *International Journal of Non-Linear Mechanics* **20**, 507–517. Domains of attraction for multiple limit cycles of coupled van der Pol equations by simple cell mapping.
15. T. Aldemir 1991 *Probabilistic Safety Assessment and Management*, *Volume* 2 (G. Apostolokis, Editor), 1431–1436. Elsevier Science Publishing Co. New York. Utilization of the cell-to-cell mapping technique to construct Markov failure models for process control systems.
16. M. Belhadj, M. Hassan and T. Aldemir 1992 *Reliability Engineering and System Safety* **38**, 219–236. On the need for dynamic methodologies in risk and reliability studies.
17. C. S. Hsu 1982 *International Journal of Applied Mechanics* **49**, 895–902. A probabilistic theory of nonlinear dynamical systems based on the cell state concept.
18. C. S. Hsu and R. S. Guttalu 1980 *Journal of Applied Mechanics* **47**, 940–948. An unraveling algorithm for global analysis of dynamical systems: an application of cell-to-cell mappings.
19. T. T. Soong and L. L. Chung 1985 See ref 17 *of Applied Mechanics* **52**, 230–232. Response cell probabilities for nonlinear random systems.

20. K. M. Shrestha and T. T. Soong 1988 *Probabilistic Engineering Mechanics* **3**, 92–97. Response probabilities of nonlinear random systems: a compartmental approach.
21. G. H. Golub and C. F. Van Loan 1989 *Matrix Computations*. London: The Johns Hopkins University Press.
22. A. Berman and R. J. Plemmons 1979 *Nonnegative Matrices in the Mathematical Sciences*. New York: Academic Press.
23. A. Berman, M. Neumann and R. J. Stern 1989 *Nonnegative Matrices in Dynamic Systems*. New York: John Wiley.

APPENDIX A: SOME PROPERTIES OF THE MATRIX Q

First one shows that $\sum_{m}^{N+1} q_{m,n} = 0$. Indeed

$$\sum_{m} q_{m,n} = q_{n,n} + \sum_{m \neq n} q_{m,n} = -\frac{1}{\nu_n} \int_{\substack{\hat{\mathbf{n}}(\mathbf{x}_s) \cdot \mathbf{f}(\mathbf{x}_s, t) > 0 \\ \mathbf{x}_s \in S_n}} \hat{\mathbf{n}}(\mathbf{x}_s) \cdot \mathbf{f}(\mathbf{x}_s, t)\, \mathrm{d}\mathbf{x}_s$$

$$+ \sum_{m \neq n} \frac{1}{\nu_n} \int_{\substack{\hat{\mathbf{n}}(\mathbf{x}_s) \cdot \mathbf{f}(\mathbf{x}_s, t) > 0 \\ \mathbf{x}_s \in S_n \cap S_m}} \hat{\mathbf{n}}(\mathbf{x}_s) \cdot \mathbf{f}(\mathbf{x}_s, t)\, \mathrm{d}\mathbf{x}_s \quad \text{(from equation (15))}$$

$$= -\frac{1}{\nu_n} \int_{\substack{\hat{\mathbf{n}}(\mathbf{x}_s) \cdot \mathbf{f}(\mathbf{x}_s, t) > 0 \\ \mathbf{x}_s \in S_n}} \hat{\mathbf{n}}(\mathbf{x}_s) \cdot \mathbf{f}(\mathbf{x}_s, t)\, \mathrm{d}\mathbf{x}_s + \frac{1}{\nu_n} \sum_{m \neq n} \int_{\substack{\hat{\mathbf{n}}(\mathbf{x}_s) \cdot \mathbf{f}(\mathbf{x}_s, t) > 0 \\ \mathbf{x}_s \in S_n \cap S_m}} \hat{\mathbf{n}}(\mathbf{x}_s) \cdot \mathbf{f}(\mathbf{x}_s, t)\, \mathrm{d}\mathbf{x}_s$$

$$= -\frac{1}{\nu_n} \int_{\substack{\hat{\mathbf{n}}(\mathbf{x}_s) \cdot \mathbf{f}(\mathbf{x}_s, t) > 0 \\ \mathbf{x}_s \in S_n}} \hat{\mathbf{n}}(\mathbf{x}_s) \cdot \mathbf{f}(\mathbf{x}_s, t)\, \mathrm{d}\mathbf{x}_s + \frac{1}{\nu_n} \int_{\substack{\hat{\mathbf{n}}(\mathbf{x}_s) \cdot \mathbf{f}(\mathbf{x}_s, t) > 0 \\ \mathbf{x}_s \in S_n}} \hat{\mathbf{n}}(\mathbf{x}_s) \cdot \mathbf{f}(\mathbf{x}_s, t)\, \mathrm{d}\mathbf{x}_s = 0$$

Now one proves that: (1) $\mathbf{Q}$ has only eigenvalues equal to zero or with a negative real part, and (2), all zero eigenvalues are non-degenerated. For this purpose, let $\mathbf{A} = \mathbf{I} + \alpha\mathbf{Q}$, where $\mathbf{I}$ is the $(N+1) \times (N+1)$ identity matrix and $0 < \alpha \leqslant \max_n |q_{n,n}|^{-1}$. Then

$$\lambda_A = 1 + \alpha\lambda_Q, \tag{A.1}$$

where λ_A and λ_Q are the eigenvalues of $\mathbf{A}$ and $\mathbf{Q}$, respectively. Since

$$q_{m,n} = \begin{cases} \geqslant 0 & \text{if } m \neq n, \\ \leqslant 0 & \text{if } m = n, \end{cases} \tag{A.2}$$

one must have $\alpha q_{n,n} \geqslant -1$ and hence it follows from the definition of $\mathbf{A}$ that the elements $a_{m,n}$ of matrix $\mathbf{A}$ are all non-negative. Also, since

$$\sum_{m=1}^{N+1} q_{m,n} = 0 \tag{A.3}$$

from above,

$$\sum_{m=1}^{N+1} a_{m,n} = \sum_{m=1}^{N+1} \delta_{m,n} + \alpha q_{m,n} = 1, \tag{A.4}$$

where $\delta_{m,n}$ is the Kronecker delta of arguments (m,n) and hence $\mathbf{A}$ is a (column) stochastic matrix.

Property (A.4) shows that the $N+1$ row vector $(1\ 1\ \cdots\ 1)$ is a left eigenvector of matrix A, associated with the eigenvalue 1. From Gershgorin's theorem [21], one knows that the eigenvalues λ_A are included in the union of the circles of center $a_{n,n}$ and of radius $\Sigma_{m=1,m\neq n}^{N+1} |a_{m,n}|$ $(n = 1, \ldots, N+1)$. Then $|\lambda_A| \leqslant 1$ and $\mathrm{Re}\,\lambda_A \leqslant 1$ and since 1 is an eigenvalue, the spectral radius $\rho(\mathbf{A})$ of $\mathbf{A}$ is 1. From equation (A.1), this result implies that: (1) $\mathbf{Q}$ has only eigenvalues equal to zero or with negative real parts and (2), there is at least one $\lambda_Q = 0$. From the Perron-Frobenius theorem, it can be also shown that [22, 23], all the eigenvalues λ_A of modulus equal to $\rho(\mathbf{A})$ $(=1)$ are non-degenerated and hence all $\lambda_Q = 0$ are non-degenerated.

APPENDIX B: AN EXAMPLE ON THE CONVERGENCE OF CONTINUOUS CCMT FOR $V_n \to 0$

Consider the system

$$\frac{\mathrm{d}x}{\mathrm{d}t} = a, \qquad x(0) = 0, \tag{B.1}$$

where $R \equiv [0, x_{max}]$. The associated probabilistic problem is

$$\partial p(x,t)/\partial t + a\,\partial p(x,t)/\partial x = 0, \qquad p(0,t) = \delta(x), \tag{B.2}$$

and its exact solution is $p(x,t) = \delta(x - at)$, $t \geqslant 0$.

Let $V_n \equiv (n-1)h < x \leqslant nh$ $(n = 1, \ldots, N)$ with $h = x_{max}/N$. From equations (14) and (15), one has

$$\frac{\mathrm{d}p_n(t)}{\mathrm{d}t} = \sum_{m=1}^{N} q_{n,m} p_m(t), \qquad p_1(0) = 1,\ p_n(0) = 0, \quad \text{for } n > 1, \tag{B.3}$$

where

$$q_{n,m} = \begin{cases} a/h & \text{if } n = m+1, \\ -a/h & \text{if } n = m, \\ 0 & \text{otherwise.} \end{cases} \tag{B.4}$$

The solution of equation (B.3) is

$$p_n(t) = [(at/h)^{n-1}\,\mathrm{e}^{-at/h}]/(n-1)!. \tag{B.5}$$

Define $\gamma = n/N$. One has to prove that $p_n(t)/h$ tends to $p(x,t)$, with $x = nh = \gamma x_{max}$, for $h \to 0$ or $N, n \to \infty$, since $(n-1)h < x \leqslant nh$ and thus $n \approx x/h$ for small h. Now integrate this function from $x = x_1$ to $x = x_2$ $(0 \leqslant x_1 < x_2)$:

$$I = \int_{x_1}^{x_2} \frac{p_n(t)}{h}\,\mathrm{d}x = \frac{1}{at}\int_{x_1}^{x_2} (atn/\xi)^n \frac{\mathrm{e}^{-atn/\xi}}{(n-1)!}\,\mathrm{d}\xi$$

$$= \frac{n}{n-1}\left[\mathrm{e}^{-u}\sum_{k=0}^{n-2}\frac{u^k}{k!}\right]_{atn/x_1}^{atn/x_2} = \frac{n}{n-1}\left(\boldsymbol{\Phi}_n(\beta_2) - \boldsymbol{\Phi}_n(\beta_1)\right), \qquad \text{where } \beta_i = atn/x_i \tag{B.6}$$

and

$$\lim_{n\to\infty} \mathbf{\Phi}_n = \lim_{n\to\infty} \left(\frac{n}{n-1} \, \mathrm{e}^{-\beta n} \sum_{k=0}^{n-2} \frac{(\beta n)^k}{k!} \right) = \begin{cases} 0, & \beta > 1, \\ 1, & \beta < 1. \end{cases}$$

Then, if $x_1 < x_2 < at$, one has $\beta_1 > \beta_2 > 1$ and $I = 0 - 0 = 0$; if $at < x_1 < x_2$, one has $1 > \beta_1 > \beta_2$ and $I = 1 - 1 = 0$; if $x_1 < at < x_2$, one has $\beta_1 > 1 > \beta_2$ and $I = 1 - 0 = 1$. I equals 1 if and only if $at \in (x_1, x_2)$ and $I = 0$ otherwise. Since the interval $x_1 < at \leqslant x_2$ can be chosen to be arbitrarily small, $p_n(t)/h$ as given by equation (B.5) corresponds for $n \to \infty$ to the definition of $\delta(x - at)$, which is the exact solution of the problem.